Above Threshold Ionization Beyond the High Harmonic Cutoff

K. J. Schafer,[1] Baorui Yang,[2] L. F. DiMauro,[2] and K. C. Kulander[1]
[1] *Lawrence Livermore National Laboratory, Livermore, California 94550*
[2] *Chemistry Department, Brookhaven National Laboratory, Upton, New York 11973*
(Received 2 December 1992)

We present high sensitivity electron energy spectra for xenon in a strong 50 ps, 1.053 μm laser field. The above threshold ionization distribution is smoothly decreasing over the entire kinetic energy range (0–30 eV), with no abrupt changes in the slope. This is in direct contrast to the sharp cutoff observed in xenon optical harmonic generation spectra. Calculations using the single active electron approximation show excellent agreement with the observed electron distributions. These results directly address the unresolved relationship between the electron and photon emission from an atom in an intense field.

PACS numbers: 31.90.+s, 32.80.Fb, 32.80.Rm

Both high-order optical harmonic generation (OHG) and above threshold ionization (ATI) occur when a bound electron absorbs many more photons from a strong laser field than the minimum number necessary for weak-field ionization. An electron that has absorbed many photons, and is possibly in the continuum, can emit one shorter wavelength photon and make an optical transition back to a lower (usually the ground) bound state (OHG), or it may ionize and emerge from the laser focus with some excess kinetic energy (ATI). Theoretical models [1, 2] have emphasized that both ATI and OHG are essentially single-atom phenomena which have their origin in the response of a single, strongly driven electron to an oscillating electric field. Therefore, one might reasonably predict that electron and photon spectra will have many similar features [2–4]. Although this issue is fundamental to the understanding of strong-field laser-atom interactions, the exact relationship between ATI and OHG has remained largely an unanswered question. This is in part due to the absence of any experiments on ATI distributions over a large dynamic range which correlate with OHG experiments. The purpose of this Letter is to address this relationship using new experimental evidence from high sensitivity electron energy measurements.

OHG spectra have a distinctive shape: a rapid decrease for the low-order harmonics consistent with perturbation theory, followed by a "plateau" region where the harmonic intensity drops more slowly, and then an abrupt *cutoff*, beyond which no harmonics are observed [5]. Because of the inversion symmetry of an atom in a linearly polarized field, only odd harmonics are produced. A simple formula predicting the harmonic cutoff was recently proposed [6] and has been verified experimentally [7]. Similarly, ATI electron spectra [8, 9] show a series of peaks separated by one photon energy. In this Letter we report ATI spectra for xenon atoms using a 50 ps, 1.053 μm laser at intensities of a few times 10^{13} W/cm^2, for which comparable OHG data [10] exist. We also present electron energy distributions from time-dependent calculations for these conditions. These same calculations were earlier found to give excellent agreement with OHG experiments [10] in xenon for the same intensity range considered here. The laser used operates at a *kilohertz* repetition rate, making it possible to measure ATI spectra over many orders of magnitude in dynamic range. We observe that the ATI spectra decrease relatively smoothly with photon order up to total energies (binding plus photoelectron energy) that are more than *twice* the reported harmonic cutoff at the same intensity. Our conclusion is that there is a striking difference between electron and photon emission. While OHG spectra have a cutoff, ATI spectra do not. Although this is contrary to an earlier prediction [2], it is in excellent agreement with the results of our calculations.

The experiment has its genesis in the calculations summarized in Fig. 1 [11]. We start with an electron wave function which is the ground state of the atomic Hamilto-

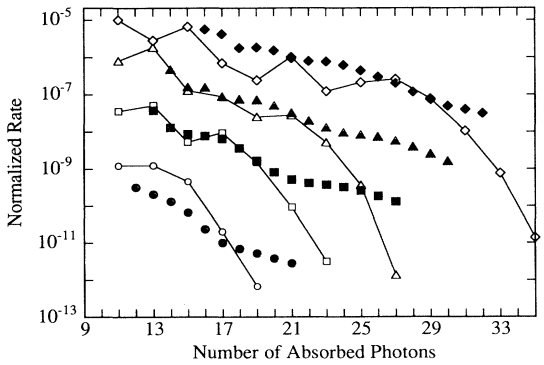

FIG. 1. The SAE model results for the "single-atom" electron (solid symbols) and photon (open symbols) emission spectrum at four different intensities: 5×10^{13} W/cm^2 (diamonds), 3×10^{13} W/cm^2 (triangles), 2×10^{13} W/cm^2 (squares), and 1×10^{13} W/cm^2 (circles). Note the sharp cutoff in the OHG spectra compared with the smooth decrease in the ATI electrons.

nian. We use the "single active electron" (SAE) approximation [12] which assumes that multiphoton ionization (MPI) occurs for one valence electron at a time in the mean field of the remaining unexcited electrons. This approach is fundamentally sound for rare gas atoms in long wavelength fields since the dominant mechanism for MPI is single electron sequential excitation. We solve the time-dependent Schrödinger equation (TDSE) on a numerical grid to follow the evolution of the active electron in the pulsed laser field. This approach makes no *a priori* assumptions about the relative strengths of the intra-atomic and the laser-atom interactions. From this single time-dependent wave function we calculate both ATI and OHG spectra [1]. These single-atom spectra can be directly compared to experiment by properly accounting for the spatial and temporal intensity variation within the laser focus, as well as propagation effects for harmonic generation.

Figure 1 shows single-atom electron and photon emission rates calculated for xenon at 1.064 μm. The small difference in wavelength between the calculations and experiment is not expected to be important at these intensities. Xenon has two possible low-lying core states when an electron is excited corresponding to $J = 3/2$ and $J = 1/2$ components of the $5p^5$ configuration of the ion. Here we show results only for the $J = 3/2$ core which has a weak-field ionization potential (I_P) of 12.13 eV. The I_P of the $J = 1/2$ core is ~ 1.3 eV higher and contributes negligibly to the ionization at these intensities. The rates are calculated for a specific intensity by using a trapezoidal pulse envelope [1]. ATI rates are given by the probability of finding the electron in a given positive energy state after the laser is off divided by the pulse length. The rate of single electron photoemission is proportional to the square of the Fourier transform of the induced time-dependent dipole at the harmonic frequency, $\sigma(q\omega) \propto (q\omega)^3 |d(q\omega)|^2$, where q is the harmonic order and ω is the laser frequency. The OHG spectrum is calculated during the latter portion of the pulse after any transients due to the turn on have decayed. The electron and photon emission rates shown in Fig. 1 have been normalized to agree for the 17-photon process at 3×10^{13} W/cm^2. The ATI curves and the OHG curves basically scale the same with intensity above 1×10^{13} W/cm^2. The most outstanding result of these calculations is that the OHG curves show a cutoff while the ATI curves continue to smoothly decrease with increasing order. The energy E_c of the single-atom OHG cutoffs can be fit by the simple rule

$$E_c \sim I_p + 3U_p\,, \tag{1}$$

where U_p is the ponderomotive energy of a free electron in a laser field of intensity I, given by $I/4\omega^2$ in atomic units [6]. This rule was proposed based upon numerical calculations in a variety of atomic and model potentials. These potentials shared only the existence of a bound state separated by several photons from a continuum. The predicted dependence has been observed to hold in several recent experiments [7]. Testing the prediction that ATI spectra do not have the same cutoff as OHG is more difficult, since ATI experiments are carried out at low gas pressures to minimize space charge effects. To follow the ATI spectrum past the harmonic cutoff requires the great sensitivity which we have been able to achieve in this experiment.

The experimental apparatus has been discussed in detail elsewhere [13]. Briefly, we use a Nd:YLF laser system based on a cw-pumped regenerative amplifier which produces 4 mJ, 50 ps pulses operating at a 1 kHz repetition rate. The output of the amplifier at 1.0527 μm runs in a TEM_{00} spatial mode with a 1% pulse-to-pulse amplitude stability. The light is focused by $f/4$ optics into an ultrahigh vacuum chamber equipped with both an electron and mass spectrometer which view the interaction region 180° apart. The electron resolution is approximately 5% of the electron energy. Electrons or ions are detected by microchannel plate detectors and their arrival times recorded by a gigahertz multihit time-to-digital converter.

We show the measured ion yields for the three lowest charge states of xenon as functions of laser intensity in Fig. 2. For comparison we have superimposed the theoretical yields for Xe^+ generated by integrating the single-atom ionization rates over the spatial and temporal intensity distribution in the focus. The ionization rates are obtained by summing the ATI rates or, alternatively, by evaluating the flux of electron density passing through a surface well removed from the atom. The calculated total ion yields agree well with the experimental curves within the measured intensity uncertainty (50%). We use the ion yields to calibrate the experimental intensity when

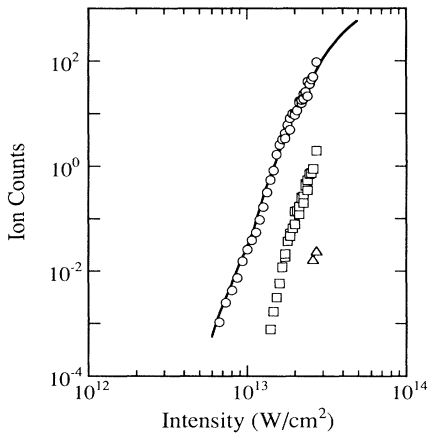

FIG. 2. A log-log plot of the experimental intensity dependence of Xe^+ (circles), Xe^{2+} (squares), and Xe^{3+} (triangles) ions, along with the spatial and temporal averaged results for Xe^+ ions from the SAE calculation (solid line).

selecting experimental ATI spectra to compare with our calculated distributions.

The semilog plot of Fig. 3 displays a sequence of photoelectron kinetic energy spectra recorded at different intensities. Spectrum 3(a) shows a well developed series of $\sim$ 22 ATI peaks extending out to 30 eV in electron energy and encompassing 5 orders of magnitude in dynamic range. The peak positions are intensity independent and fit an $(11 + S)\hbar\omega - I_P$ progression, where S is the number of ATI photons, and the photon energy is $\hbar\omega = 1.17$ eV. The normalized ordinate is the total number of electrons collected in 7.2×10^6 laser shots at a xenon density of $2 \times 10^{10}/\text{cm}^3$. The maximum count rate used is one electron per shot which equates to 50 xenon ions in the interaction volume. The high repetition rate of the laser enables the efficient collection of electron counts while minimizing the effects of space charge. In fact, space charge limitations make this experiment virtually impossible using low repetition rate sources. The overall shape of the ATI peak distribution has been carefully checked at different xenon densities and found to give consistent results. The ATI spectra shown in Fig. 3 show no evidence of any abrupt cutoff. As the intensity is increased the number of high energy ATI peaks visibly increases while the low energy electrons are ponderomotively suppressed, but the overall slope remains approximately constant. This is clearly seen in Fig. 4 where we plot the integrated counts for each ATI peak as a function of the number of absorbed photons. Also in Fig. 4 we plot the results of our SAE calculations for the same peak intensity, normalized to agree for the 24-photon process at 2×10^{13} W/cm^2. We compare calculations at the same peak intensity, without a spatial integration over the laser focus, which is valid below saturation given the nonlinearity of the MPI process. There is excellent agreement with the smooth falloff of the experimental points and with the overall intensity dependence.

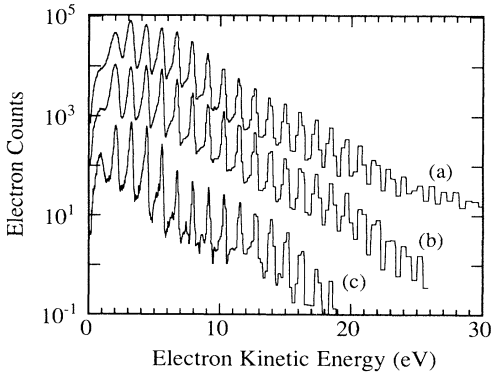

FIG. 3. A semilog plot of the photoelectron kinetic energy spectrum of xenon using 50 ps, 1.05 μm excitation. The intensities used are (a) 2×10^{13} W/cm^2, (b) 1.5×10^{13} W/cm^2, and (c) 1×10^{13} W/cm^2. The absolute counts are normalized and a typical data set consists of 7.2×10^6 laser shots.

While the ATI results can be compared almost directly to experiment, the single-atom OHG spectra cannot for two reasons. First, even though the induced dipole due to excitations outside the $J = 1/2$ ion core is generally much smaller than those involving the $J = 3/2$ core, the two must be added coherently because photons from the two sources cannot be distinguished. Consequently, the resulting cross term may not be negligible. Second, the observation of OHG requires phase matching of the generated harmonic fields [10]. Calculations for strong laser fields reveal that phase matching has only a weak effect on the harmonics in the plateau region. This is due to the uniform scaling of the single-atom harmonics with intensity, seen in Fig. 1. Single-atom harmonics beyond the plateau rise steeply with intensity leading to poor phase matching. This effect, combined with the much weaker emission strengths, leads to a sharp cutoff in the experimental (macroscopic) spectrum. Therefore, the experimental OHG spectra, while not identical to single-atom spectra, share the same basic features, i.e., a plateau and cutoff. In particular, the location of the cutoff in the single-atom spectrum predicts the experimental cutoff quite accurately [7, 10]. Previous xenon experiments have found the highest OHG cutoff for 36 ps, 1.06 μm pulses (saturation intensity $\sim 3 \times 10^{13}$ W/cm^2) to be no higher than the 21st order, in agreement with Fig. 1. This corresponds to $\sim$ 12 eV electron kinetic energy in Fig. 3 or 21 photons in Fig. 4.

Our results demonstrate that any theory of multiphoton processes must explain the existence of a cutoff in the harmonic spectrum at $\sim I_p + 3U_p$ and the absence of an ATI cutoff. The intrinsic difference between ATI and OHG can be appreciated by considering a "two step"

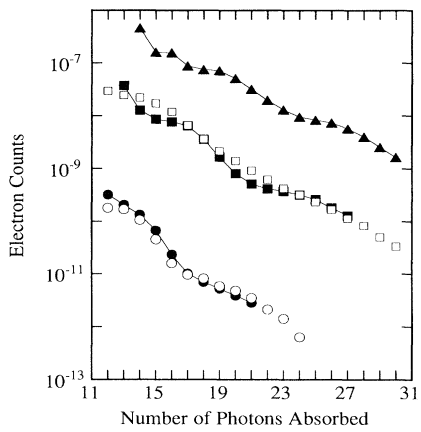

FIG. 4. A semilog plot of electron yield vs the number of absorbed photons. The intensities are 1×10^{13} W/cm^2 (circles), 2×10^{13} W/cm^2 (squares), and 3×10^{13} W/cm^2 (triangle; theory only). The open symbols are the peak-integrated value derived from the experimental ATI spectra of Fig. 3. The solid-line–symbol combination are the electron emission results obtained for the $J = 3/2$ Xe core using the SAE model.

semiclassical model. In the first step, electrons are released near the nucleus via either tunneling or multiphoton absorption during each optical cycle [14]. The subsequent evolution of these electrons can be treated classically. We find two types of classical orbits: those that return to the region near the nucleus and those that do not. The ATI energy is equated with the drift velocity that the newly freed electron gains from the field. The drift velocity, which is a *cycle-averaged quantity*, varies depending upon the phase of the electric field when the free electron is born. For electrons that are born with zero initial kinetic energy, the maximum drift velocity corresponds to measured energies of $3U_p$ in the long pulse limit. Additional drift velocity, resulting in energies substantially higher than $3U_p$, can be gained if the electron is born with some initial kinetic energy, or if it has a collision with the nucleus. This gives a likely source of the high energy electrons observed. OHG occurs only for those orbits which have at least one additional collision with the nucleus. This is borne out by numerical calculations which show that high-order harmonic production is completely accounted for by considering only transitions that end in the ground state [1]. Therefore, the maximum energy that the emitted photon can have must be the energy that the electron has *at the time it revisits the vicinity of the nucleus.* We find that for electrons that are born near the nucleus, regardless of their initial energy distribution, the maximum energy at the return time is 3.17 U_p plus the field free ionization potential. This predicts the OHG cutoff remarkably well. The distinction between averaged and instantaneous energies is the key difference between ATI and OHG.

In summary, we have presented an experimental study of xenon atoms in strong laser fields that illuminates some aspects of the relationship between above threshold ionization and harmonic generation from a single atom. The agreement between the theoretical and experimental results illustrates the ability of the SAE model to describe multiphoton processes in multielectron atoms. It also reinforces the assumption that the excitation dynamics responsible for the observed electron and photon emission are dominated for the rare gases by single electron excitation processes.

We wish to acknowledge helpful conversations with Anne L'Huillier and Jeffrey Krause. This research was carried out in part at Brookhaven National Laboratory under Contract No. DE-AC02-76CH00016 with the U.S. Department of Energy and supported by its Division of Chemical Sciences, Office of Basic Energy Sciences, and in part under the auspices of the U.S. Department of Energy at Lawrence Livermore National Laboratory under Contract No. W-7405-ENG-48.

[1] K. J. Schafer, J. L. Krause, and K. C. Kulander, Int. J. Nonlinear Opt. Phys. **1**, 245 (1992).
[2] J. H. Eberly, Q. Su, and J. Javanainen, Phys. Rev. Lett. **62**, 881 (1989).
[3] B. W. Shore and P. L. Knight, J. Phys. B **20**, 413 (1987).
[4] F. H. M. Faisal, in *Atoms in Strong Fields*, edited by C. A. Nicolaides, C. W. Clark, and M. H. Nayfeh (Plenum, New York, 1990), p. 407.
[5] X. F. Li, A. L'Huillier, M. Ferray, L. A. Lompré, and G. Manus, Phys. Rev. A **39**, 5751 (1989).
[6] J. L. Krause, K. J. Schafer, and K. C. Kulander, Phys. Rev. Lett. **68**, 3535 (1992); Phys. Rev. A **45**, 4998 (1992).
[7] A. L'Huillier and P. Balcou, Phys. Rev. Lett. **70**, 774 (1993); J. J. Macklin, J. D. Kmetic, and C. L. Gordon III, *ibid.* **70**, 766 (1993); J. K. Crane, M. D. Perry, S. Herman, and R. W. Falcone, Opt. Lett. **18**, 1256 (1992).
[8] P. Agostini, F. Fabre, G. Mainfray, G. Petite, and N. K. Rahman, Phys. Rev. Lett. **42**, 1127 (1979).
[9] R. R. Freeman, P. H. Bucksbaum, and T. J. McIlrath, IEEE J. Quantum Electron. **24**, 1461 (1988).
[10] A. L'Huillier, K. J. Schafer, and K. C. Kulander, Phys. Rev. A **46**, 2778 (1992).
[11] K. C. Kulander, K. J. Schafer, and J. L. Krause, in *OSA Proceedings on Short-Wavelength Coherent Radiation*, edited by P. H. Bucksbaum and N. M. Ceglio (Optical Society of America, Washington, DC, 1991).
[12] K. C. Kulander, K. J. Schafer, and J. L. Krause, Int. J. Quantum Chem. Quantum Chem. Symp. **25**, 415 (1991).
[13] M. Saeed, D. Kim, and L. F. DiMauro, Appl. Opt. **29**, 1752 (1990); L. F. DiMauro, D. Kim, M. W. Courtney, and M. Anselment, Phys. Rev. A **38**, 2338 (1988).
[14] P. B. Corkum, N. H. Burnett, and F. Brunel, Phys. Rev. Lett. **62**, 1259 (1989). Corkum has independently extended the quasistatic model along the lines described here (to be published).